Supporting Information

Crystalline Copper (II) Phthalocyanine Catalysts for Electroctrochemical Reduction of Carbon Dioxide in Aqueous Media

Shoko Kusama*, Teruhiko Saito, Hiroshi Hashiba, Akihiro Sakai, Satoshi Yotsuhashi

†Advanced Technology Research Laboratory, Panasonic Corporation, Kyoto 619-0237, Japan

kusama.shoko@jp.panasonic.com

1. Materials

Copper phthalocyanine (CuPc) and its derivatives, 2,9,16,23-tetra-*tert*-butylphthalocyanine copper [$(tBu)_4$CuPc], 2,3,9,10,16,17,23,24-octafluorophthalocyanine copper (F_8CuPc), 1,2,3,4,8,9,10,11,15,16,17,18,22,23,24,25-hexadecafluorophthalocyanine copper (F_{16}CuPc), and 5,9,14,18,23,27,32,36-octabutoxy-2,3-naphthalocyanine copper [$CuNc(BuO)_8$] were purchased from Tokyo Chemical Industry Co., Ltd., and used without further purification. Carbon black (Vulcan XC-72R) was purchased from Cabot Corporation. Glassy carbon rods were purchased from Toyo Tanso Co., Ltd., and always washed and sonicated in acetone before depositing catalysts. Mili-Q water (Merck Millipore Co., Bedford, MA) was used in all the experiments.

Chart S1. Series of CuPc derivatives

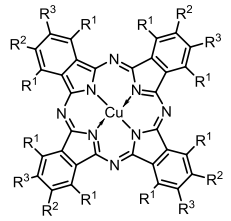

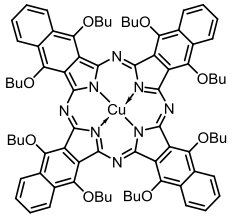

2. Experimental section

Preparation of carbon-supported CuPc

Carbon-supported crystalline CuPc and its derivatives were prepared by mixing carbon black with CuPc powder (150 mg (12.5 mmol) carbon and 66 mg (0.12 mmol)) in *N*,*N*-dimethyformamide. After evaporation of the solvent, the obtained powder was vacuum dried to give CuPc/C catalysts. Carbon-supported crystalline CuPc derivatives were also prepared by similar method using ethanol as a solvent instead of *N*,*N*-dimethyformamide.

Preparation of carbon-supported CuPc electrodes

Crystalline CuPc/C electrodes (0.3 μmol copper/cm^2, 32-37 μmol carbon/cm^2, and 124 μg Nafion®/cm^2) were prepared as follows: carbon-supported CuPc and its derivatives (8.5 mg, except for $CuNc(BuO)_8$ (12 mg)) were dissolved in 426 μl of acetone containing 37.1 μl of Nafion® perfluorinated resin solution (5 wt. % in lower aliphatic alcohols and water, contains 15-20 % water, Sigma-Aldrich) and the suspension was sonicated to form homogenous ink. Then 27.7 μl of the ink solutions were pipetted onto glassy carbon rods (Toyo Tanso, 10 mm in diameter and 8 mm in length) followed by immediate evaporation of solvents either at room temperature or vacuum drying. The glassy carbon rods were attached to aluminum sheets via DOTITE D-723S (FUJIKURA KASEI CO., LTD, Japan), and supported by glass substrates. In the case of the preparation of $CuNc(BuO)_8$/C electrode, 161 μg Nafion®/cm^2 was used.

Preparation of noncrystalline CuPc and its electrode

CuPc and its derivatives powder (250 mg, 0.43 mmol) were added to 10 ml of sulfuric acid, and the solution was stirred for 1 h. The obtained solution was then dropped to 25 ml of ethyl acetate, and mixed for another 30 min. The suspension was finally filtrated and washed with ethyl acetate, followed by vacuum drying at 90°C and pulverization with a mortar and pestle, giving dark green powder. The crystallinity of the powder was recognized by X-ray diffraction analysis.

Noncrystalline CuPc/C electrodes (0.3 μmol copper/cm^2, 37 μmol carbon/cm^2, and 124 μg Nafion®/cm^2) were prepared as described in the previous section. As to CuPc derivatives, non-crystallinity could not be confirmed in all of them; therefore, we just call the derivatives "H_2SO_4-trearted" catalysts.

Recovering the crystallinity of CuPc

Noncrystalline CuPc was then sonicated and incubated at 80°C firstly in Mili-q water and secondly in chloroform to restore its crystallinity. After evaporation of the solvent, blue powder was obtained. The crystallinity of the powder was recognized by X-ray diffraction analysis.

X-ray diffraction analysis (XRD)

X-ray diffractometer (RINT-TTR III, Rigaku) using Cu-Kα radiation at 50 kV/300 mA, and scanning electron microscopy (SU8220, Hitachi, Ltd, Japan) were used to analyze crystallinity and surface morphology, respectively, of the CuPc/C catalysts.

Cyclic voltammetry (CV)

CV measurements in aqueous solutions (Figure 2 and S2) were performed with a two-compartment cell, using potentiostat HZ-5000 (Hokuto Denko Ltd, Japan). Ag/AgCl electrodes purchased from BAS (Japan) were used as reference. Iridium oxide (IrO_2) was used as counter electrode on the purpose of improving the efficiency of overall electrochemical reaction [1].

0.5 mol/L KCl and 0.5 mol/L $KHCO_3$ were used as catholyte and anolyte, respectively, which were separated by Nafion 117 (DuPont). CV measurements were performed after bubbling either N_2 (at a flow rate of 200 ml/min) or CO_2 (at a flow rate of 400 ml/min) into catholyte at least for 30 min. The representative voltammograms were taken from 3rd scan.

CV measurements in organic solvent (Figure S3) were performed with an one-compartment cell. A Ag/Ag^+ electrode purchased from BAS (Japan) and a platinum (Pt) wire were used as reference and counter electrodes, respectively. 0.1 mol/L tetrabutylammonium perchlorate (TBAP) in *N*,*N*-dimethylformamide (DMF) was used as electrolyte. CV measurements were performed after bubbling either Ar (at a flow rate of 200 ml/min) or CO_2 (at a flow rate of 200 ml/min) into electrolyte at least for 10 min. The representative voltammograms were taken from 6th scan.

Electrochemical CO_2 reduction

The Combi-system [2] was used for CO_2 reduction experiments shown in Figure S4, S5, S8, and S9. The Combi-system, which is more tightly sealed compared to the ordinary two-compartment cell, was used when relatively high pressure is applied to the cell due to generation of H_2, CO, and other products from electrolysis. Ag/AgCl reference electrodes were purchased form Corr instruments (TX, USA), and Pt wires as counter electrodes were purchased from BAS (Japan). 0.5 mol/L KCl and 3.0 mol/L $KHCO_3$ were used as catholyte and anolyte, respectively, which were separated by Nafion 424 (Aldrich, MO, USA). After bubbling N_2 and CO_2 (at a flow rate of 125 ml/min) into catholyte for 1 h each, cells were sealed and electrolysis was performed under CO_2-saturated condition.

The two-compartment cell mentioned in the last section was used in CO_2 reduction experiments shown in figures other than Figure S4, S5, S8, and S9.

Identification and quantification of CO_2 reduction products

Gas samples were analyzed either automatically by 7890A (Agilent, CA, United States) or manually by GC-4000 (GL Science inc., Japan) gas chromatography instruments (GC). Liquid samples were manually extracted and analyzed by a Prominemce (Shimadzu, Japan) high-performance liquid chromatography (HPLC) and a GC-17A (Shimadzu, Japan) with a TurboMatrix40 (PerkinElmer, MA, United States) headspace system (HS-GC).

Faradaic efficiency (η_F) of each product was calculated as follows:

$$\eta_F = nFN / q_t$$

, where n is the amount of each product [mol], F is faraday constant (9.65×10^4 [C mol^{-1}]), N is the number of electrons required for the formation of one molecule of each product from CO_2, and q_t is the total charge [C]. Note that due to our protocol used in the Combi-system, values of total faradaic efficiency were 100 $\pm$ 10 %.

Partial current density (j) of each product was calculated as follows:

$$j = j_{total} \times \eta_F$$

, where j_{total} is the average total current density [mA/cm^2] during electrolysis.

Amount of $^{12}C_2H_4$ and $^{13}C_2H_4$ were determined by measuring total ion current chromatograms with GCMS-QP2010SE (Shimadzu Ltd, Japan).

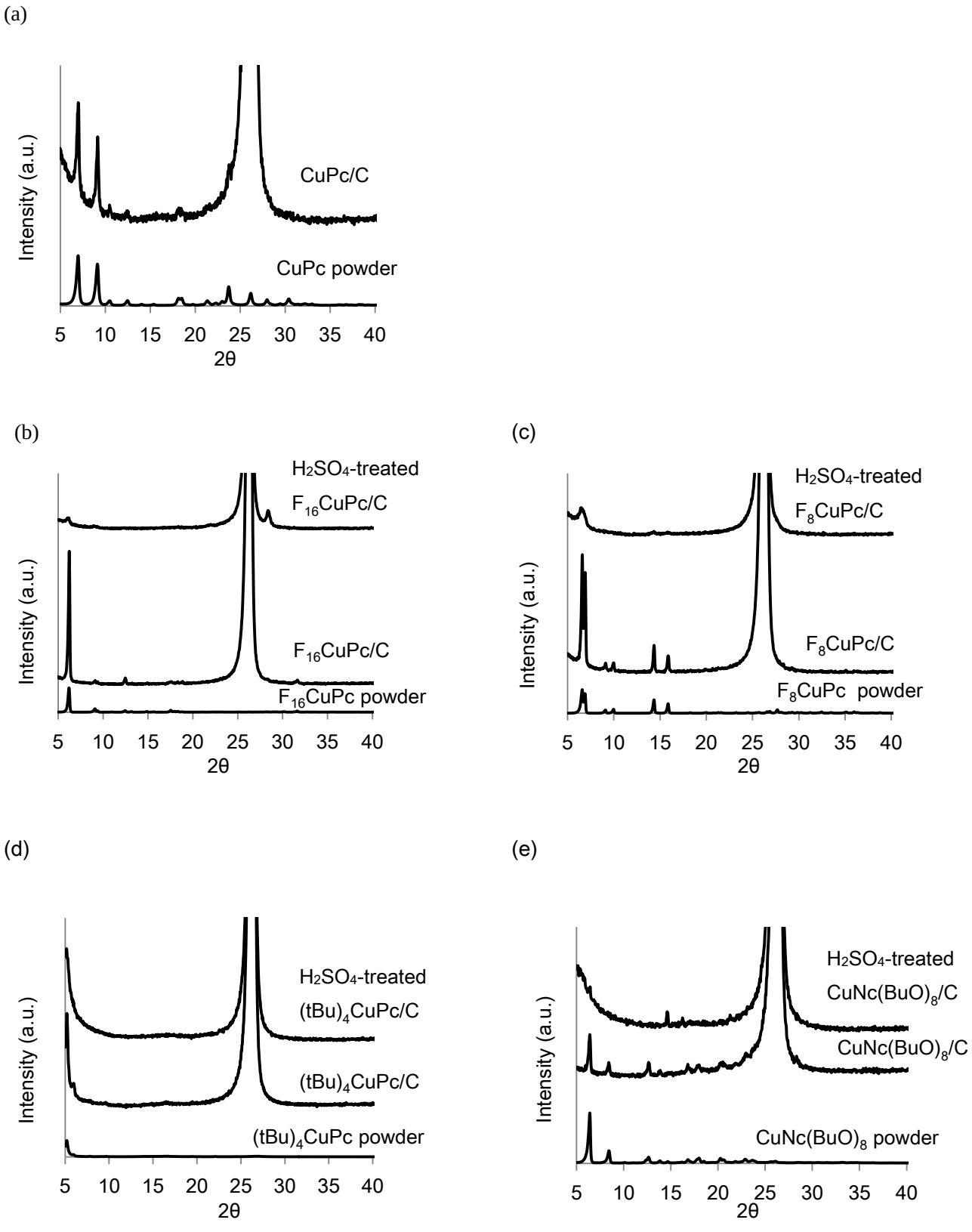

Figure S1. XRD measurements of CuPc/C (a), F_{16}CuPc/C (b), F_8CuPc/C (c), $(tBu)_4$CuPc/C (d), and CuNc$(BuO)_8$/C (e) electrodes. XRD data of H_2SO_4-treated carbon-supported CuPc derivatives are also shown except for that of CuPc/C, which is shown in Figure 3(c). On the bottom are XRD patterns of corresponding CuPc powder.

3. Discussion about crystal structure of CuPc derivatives

We considered the crystal structure of CuPc derivatives might be not so different based on the XRD spectra. Every carbon-supported CuPc derivative has relatively low-angle peaks in XRD spectra at similar positions as shown in Figure S1, indicating that every CuPc derivative has similar edge-on packing structure. However, we could not observe the peaks around at $2\theta=25°$, which reflects face-on packing in the crystal structure, due to the overlap peaks of glassy carbon substrate as shown in Figure S1.

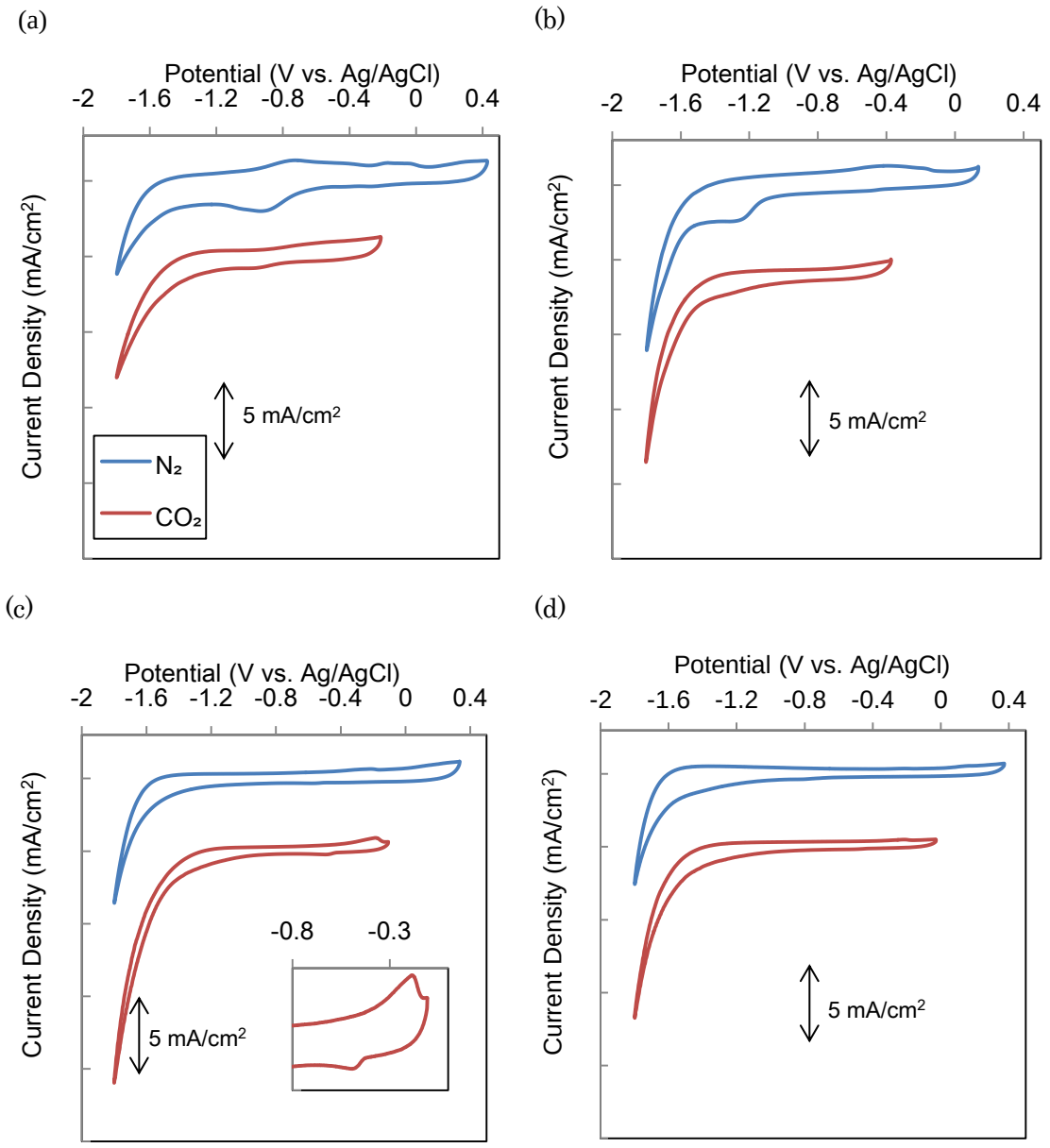

Figure S2. Cyclic voltammograms of $F_{16}CuPc/C$ (a), F_8CuPc/C (b), $(tBu)_4CuPc/C$ (c), and $CuNC(BuO)_8$ (d) measured in 0.5 M KCl under under N_2 and CO_2 atmosphere at scan rate of 50 mV s^{-1}.

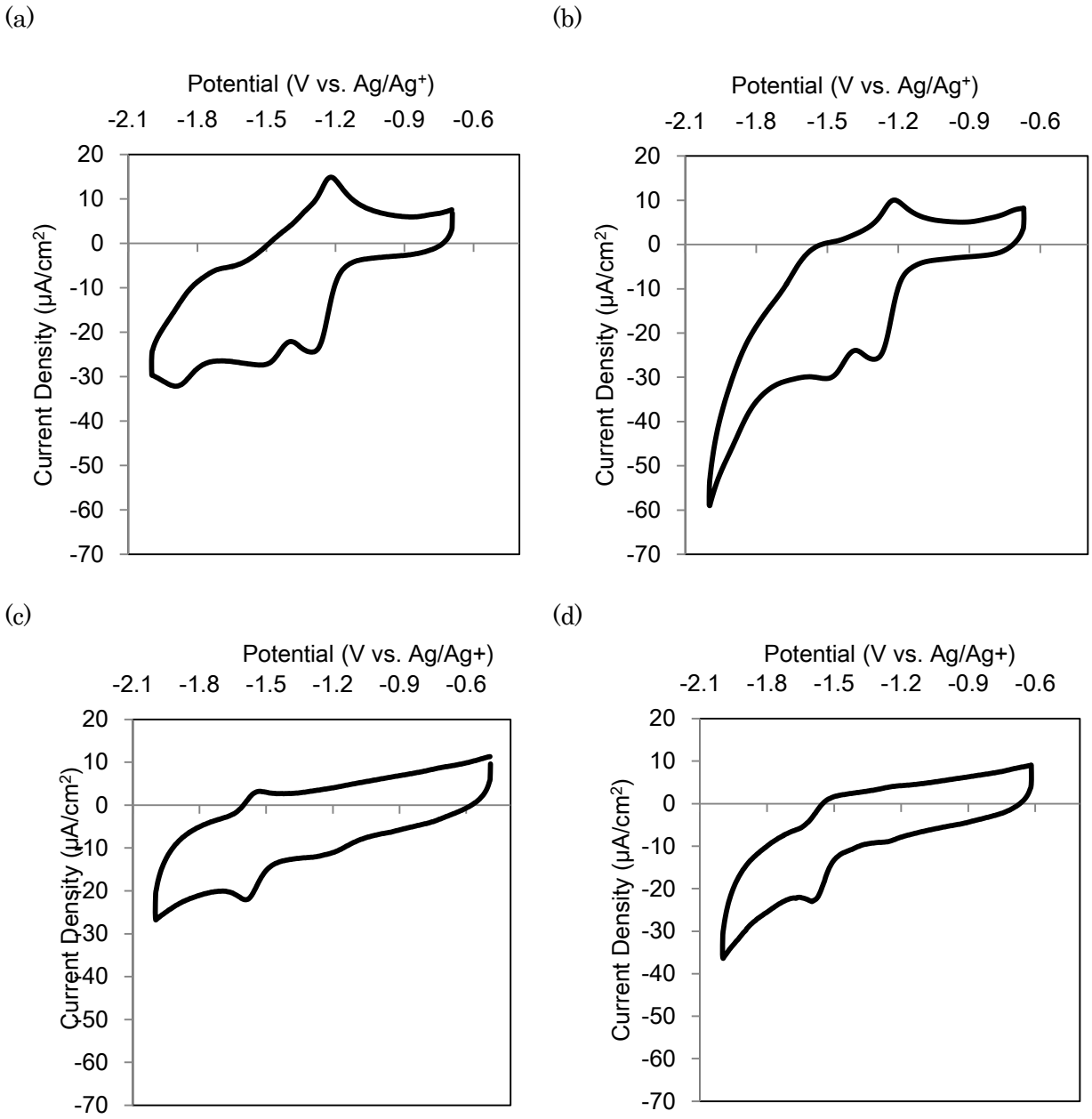

Figure S3. Cyclic voltammograms of $(tBu)_4CuPc$ measured in DMF containing 0.1 M TBAP under Ar (a) and CO_2 atmosphere at scan rate of 50 mV s^{-1} (b). CVs of Phthalocyanine without Cu were also measured under Ar (c) and CO_2 (d).

Among CuPc/C catalysts, only $(tBu)_4CuPc$ was soluble enough to be used as homogenous catalysts. Reduction processes of Cu center of $(tBu)_4CuPc$ could be clearly detected under Ar at around -1.3 V, -1.5 V and -1.9 V vs Ag/Ag^+ (a). Under CO_2, the potentials of first two waves are equal to -1.3 V and -1.5 V vs Ag/Ag^+ (b); in aqueous electrolyte, the onset potential of CO_2 reduction is around -1.5 V vs Ag/AgCl (Figure 2 and S2). Since phthalocyanine without Cu does have weaker but similar redox waves (c,d), we could only conclude that change from CuPc to $[CuPc]^-$ occurred. Therefore, reduction of CO_2 might be catalyzed by $[CuPc]^-$ or $[CuPc]^{2-}$ species in our system.

4. Discussion about substituent effect of ligands (Figure S4)

We considered that substituents on the ligands did not influence product distribution but current density though reaction mechanism was still unclear. Firstly, their crystallinity might affect the product distribution of C_2H_4 and CH_4 because CuPc molecular should be located close to each other to form C-C bonds. Based on the XRD measurements of crystalline CuPc derivatives (Figure S1), sharp peaks derived from the edge-on packing structure were commonly observed, indicating that the orientation of active sites, copper, is not significantly different from each other. Thus, CuPc derivatives gave almost the same product distribution (C2/C1 = 1.5), though CuPc showed best C2/C1 value among CuPc derivatives. Secondly, we thought the different electron states among CuPc derivatives might influence current density. In the previous report about reaction mechanism of reduction of CO_2 to form CH_4, rate-limiting step for the reaction was electron transfer and protonation of CO absorbed on Cu surface to give CHO species. Thus, not only electron density but also acidity of substrate on Cu center is quite important to give high current density in reduction of CO_2. Although the reaction mechanism is still unclear, electron transfer process and protonation might be included in rate limiting step. CuPc might possess the most desirable electron density in the reaction mechanism in our experimental conditions.

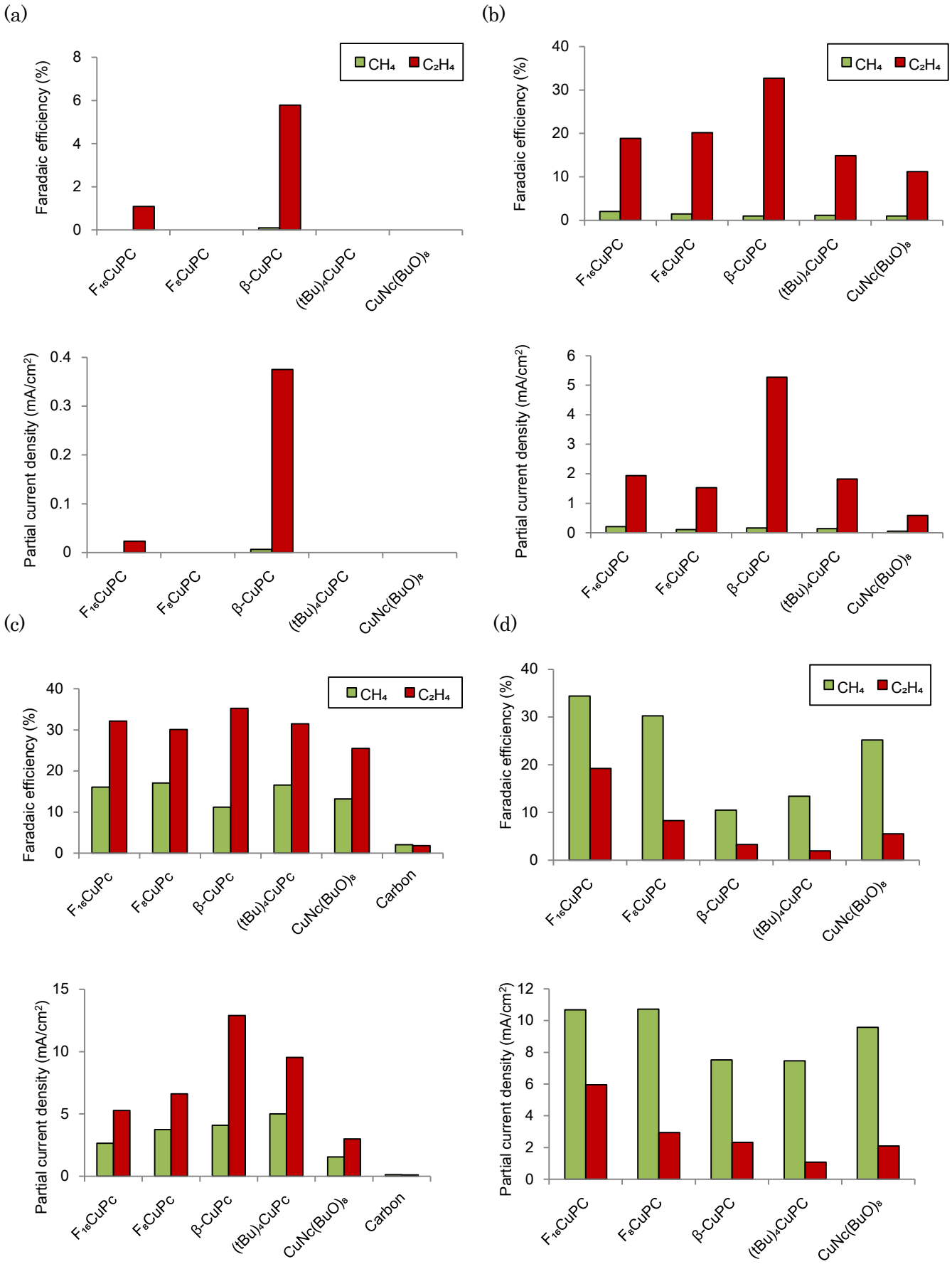
(a)
(b)
(c)
(d)
CH4
C2H4
Faradaic efficiency (%)
Partial current density (mA/cm2)
F16CuPC
F8CuPC
β-CuPC
(tBu)4CuPC
CuNc(BuO)8
Carbon

(e)

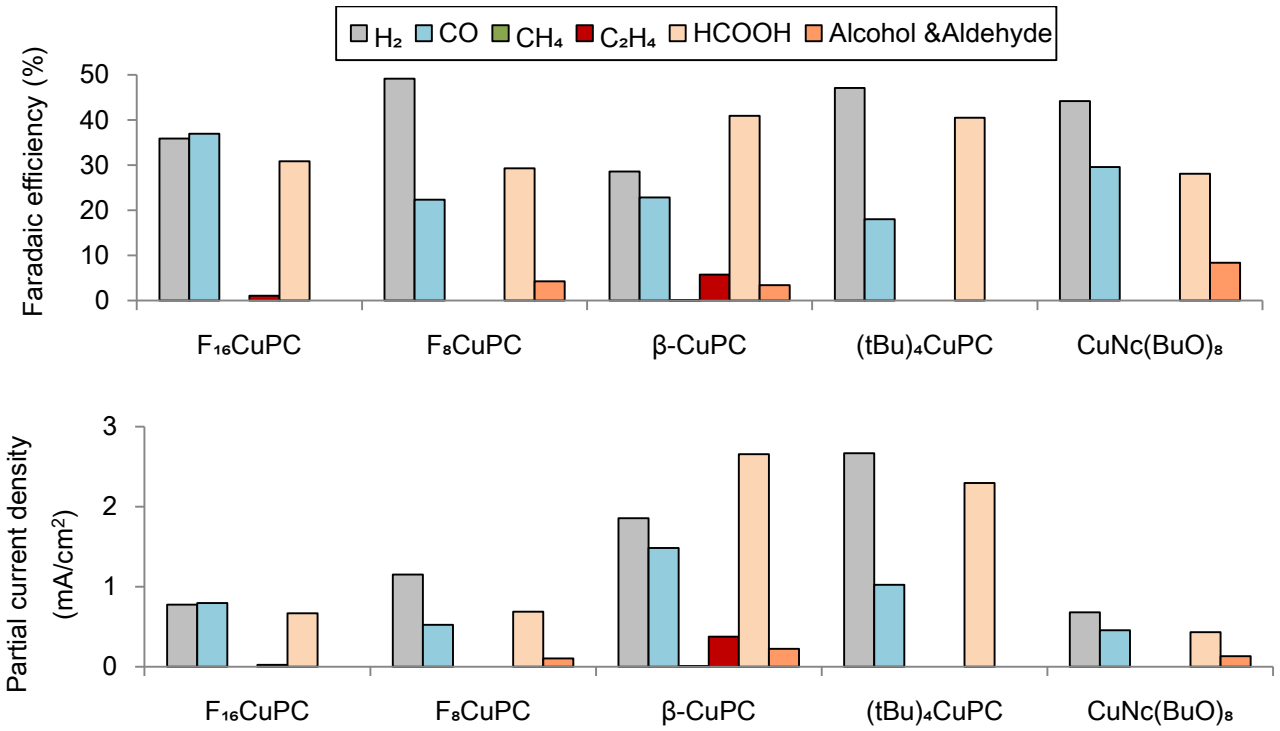
H₂
CO
CH₄
C₂H₄
HCOOH
Alcohol &Aldehyde
Faradaic efficiency (%)
50
40
30
20
10
0
F₁₆CuPC
F₈CuPC
β-CuPC
(tBu)₄CuPC
CuNc(BuO)₈
Partial current density (mA/cm²)
3
2
1
0
F₁₆CuPC
F₈CuPC
β-CuPC
(tBu)₄CuPC
CuNc(BuO)₈

(f)

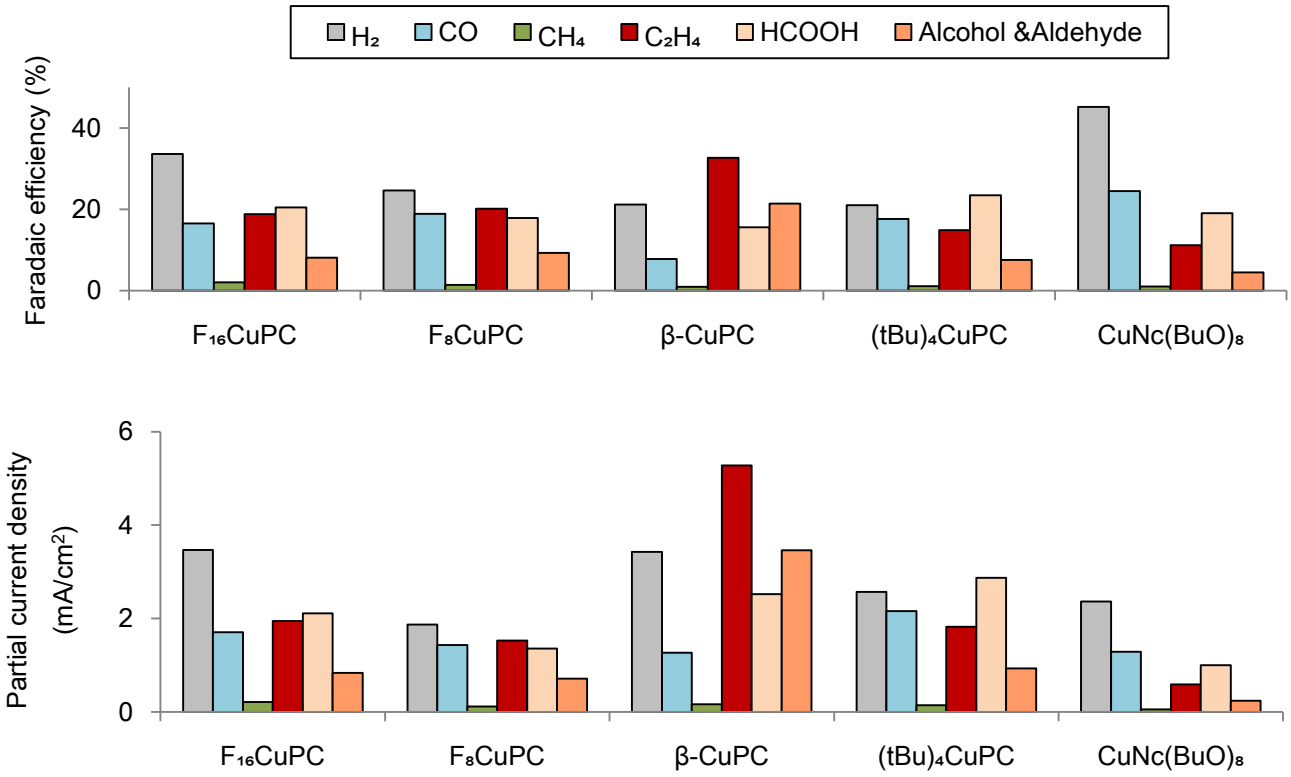
H₂
CO
CH₄
C₂H₄
HCOOH
Alcohol &Aldehyde
Faradaic efficiency (%)
40
20
0
F₁₆CuPC
F₈CuPC
β-CuPC
(tBu)₄CuPC
CuNc(BuO)₈
Partial current density (mA/cm²)
6
4
2
0
F₁₆CuPC
F₈CuPC
β-CuPC
(tBu)₄CuPC
CuNc(BuO)₈

(g)

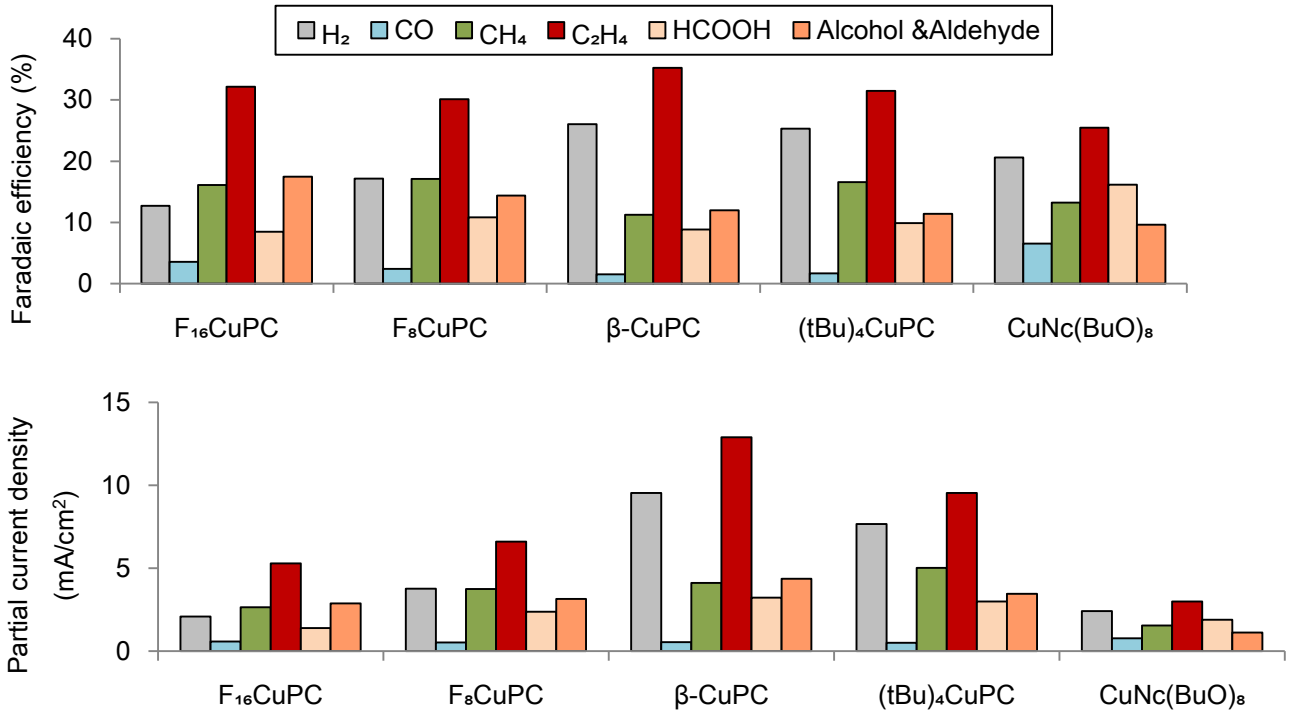

(h)

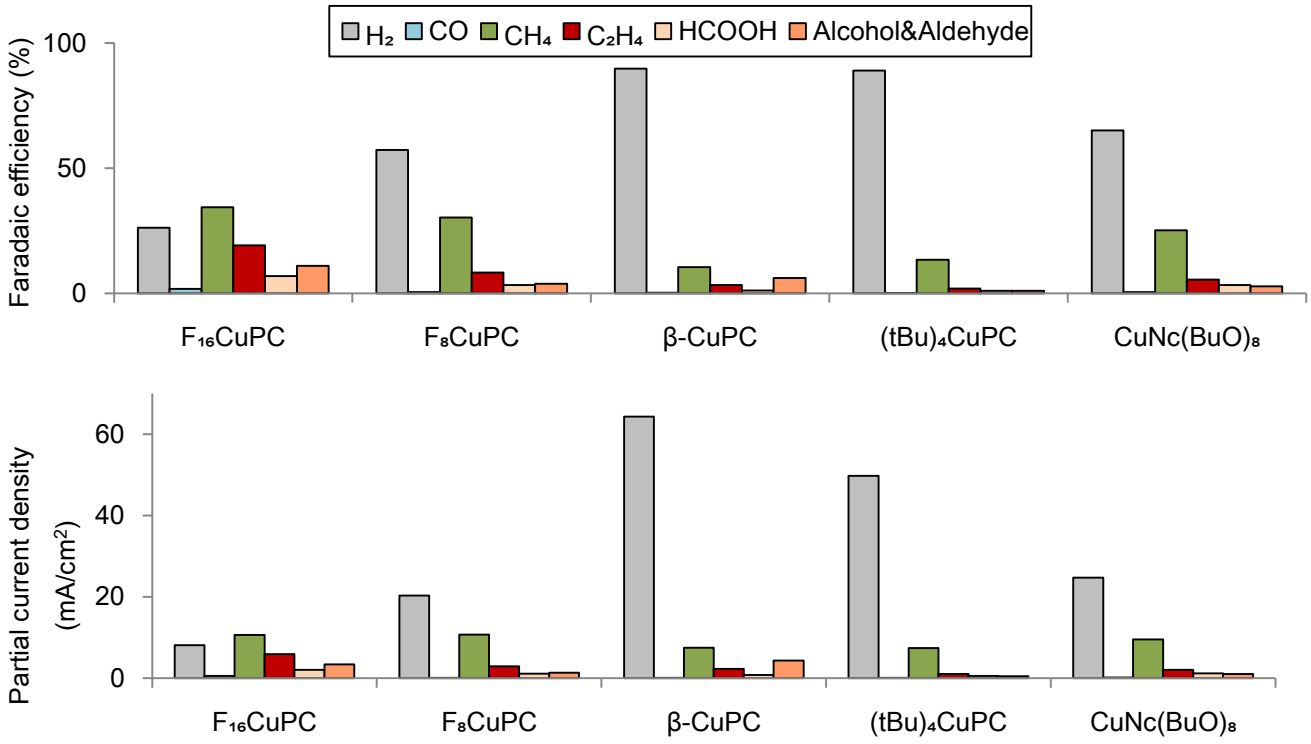

Figure S4. Faradaic efficiency and partial current density of CH_4 and C_2H_4 during electrolysis at -1.5 V (a), -1.6 V (b), -1.7V (c), and -1.8 V vs Ag/AgCl in the Combi-system (d). The overall distribution of the products from CO_2 reduction at -1.5 V (e), -1.6 V (f), -1.7 V (g), and -1.8 V vs Ag/AgCl in the Combi-system are also presented (h). N=1.

Table S1. Faradaic efficiency and partial current density of the products obtained from CO_2 reduction at -1.5 V (a), -1.6 V (b), -1.7V (c), and -1.8V vs Ag/AgCl in the Combi-system shown in Figure S4 (n=1) (d).

(a)

Faradaic efficiency (%)

	H_2	CO	CH_4	C_2H_4	HCOOH	Alcohol &Aldehyde
$F_{16}CuPc$	36	37	0	1	31	0
F_8CuPc	49	22	0	0	29	4
CuPc	29	23	0	6	41	3
$(tBu)_4CuPc$	47	18	0	0	41	0
$CuNc(BuO)_8$	44	30	0	0	28	8

Partial current density (mA/cm^2)

	H_2	CO	CH_4	C_2H_4	HCOOH	Alcohol &Aldehyde
$F_{16}CuPc$	0.8	0.8	0	0	0.7	0
F_8CuPc	1.1	0.5	0	0	0.7	0.1
CuPc	1.9	1.5	0	0.4	2.7	0.2
$(tBu)_4CuPc$	2.7	1.0	0	0	2.3	0
$CuNc(BuO)_8$	0.7	0.5	0	0	0.4	0.1

(b)

Faradaic efficiency (%)

	H_2	CO	CH_4	C_2H_4	HCOOH	Alcohol &Aldehyde
F_{16}CuPc	34	17	2	19	20	8
F_8CuPc	25	19	1	20	18	9
CuPc	21	8	1	33	16	21
$(tBu)_4$CuPc	21	18	1	15	23	8
CuNc$(BuO)_8$	45	25	1	11	19	5

Partial current density (mA/cm^2)

	H_2	CO	CH_4	C_2H_4	HCOOH	Alcohol &Aldehyde
F_{16}CuPc	3.5	1.7	0.2	1.9	2.1	0.8
F_8CuPc	1.9	1.4	0.1	1.5	1.4	0.7
CuPc	3.4	1.3	0.2	5.3	2.5	3.5
$(tBu)_4$CuPc	2.6	2.2	0.1	1.8	2.9	0.9
CuNc$(BuO)_8$	2.4	1.3	0.1	0.6	1.0	0.2

(c)

Faradaic efficiency (%)

	H_2	CO	CH_4	C_2H_4	HCOOH	Alcohol &Aldehyde
$F_{16}CuPc$	13	4	16	32	8	17
F_8CuPc	17	2	17	30	11	14
CuPc	26	1	11	35	9	12
$(tBu)_4CuPc$	25	2	17	31	10	11
$CuNc(BuO)_8$	21	7	13	25	16	10

Partial current density (mA/cm^2)

	H_2	CO	CH_4	C_2H_4	HCOOH	Alcohol &Aldehyde
$F_{16}CuPc$	2.1	0.6	2.6	5.3	1.4	2.9
F_8CuPc	3.8	0.5	3.8	6.6	2.4	3.2
CuPc	9.5	0.5	4.1	12.9	3.2	4.4
$(tBu)_4CuPc$	7.7	0.5	5.0	9.5	3.0	3.5
$CuNc(BuO)_8$	2.4	0.8	1.5	3.0	1.9	1.1

(d)

Faradaic efficiency (%)

	H_2	CO	CH_4	C_2H_4	HCOOH	Alcohol &Aldehyde
$F_{16}CuPc$	26	2	34	19	7	11
F_8CuPc	57	0	30	8	3	4
CuPc	90	0	11	3	1	6
$(tBu)_4CuPc$	89	0	13	2	1	1
$CuNc(BuO)_8$	65	0	25	6	3	3

Partial current density (mA/cm^2)

	H_2	CO	CH_4	C_2H_4	HCOOH	Alcohol &Aldehyde
$F_{16}CuPc$	8.1	0.6	10.7	6.0	2.1	3.4
F_8CuPc	20.3	0.1	10.7	2.9	1.2	1.3
CuPc	64.3	0.1	7.5	2.3	0.8	4.4
$(tBu)_4CuPc$	49.7	0.1	7.5	1.1	0.6	0.5
$CuNc(BuO)_8$	24.7	0.2	9.6	2.1	1.2	1.0

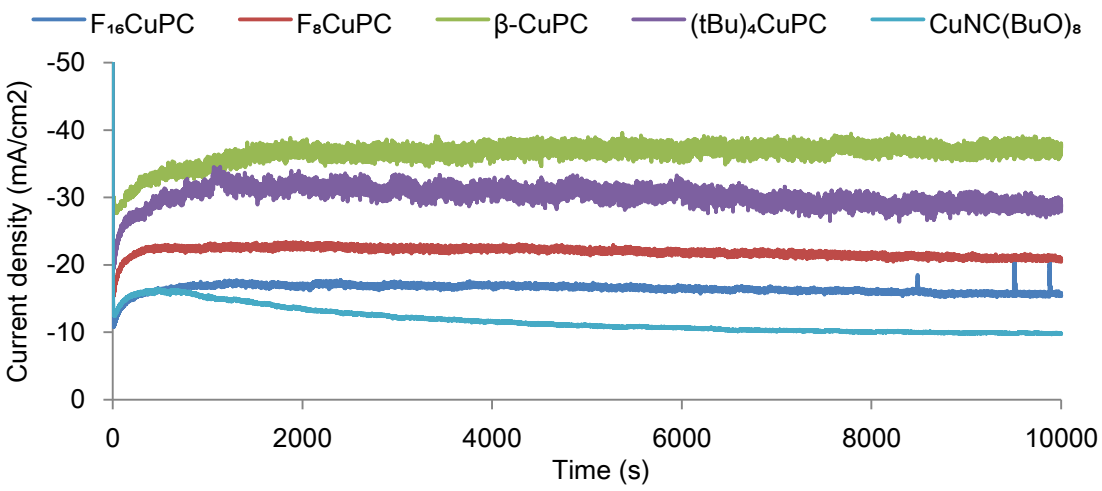

Figure S5. Changes in total current density during electrolysis at -1.7 V vs Ag/AgCl in the Combi-system.

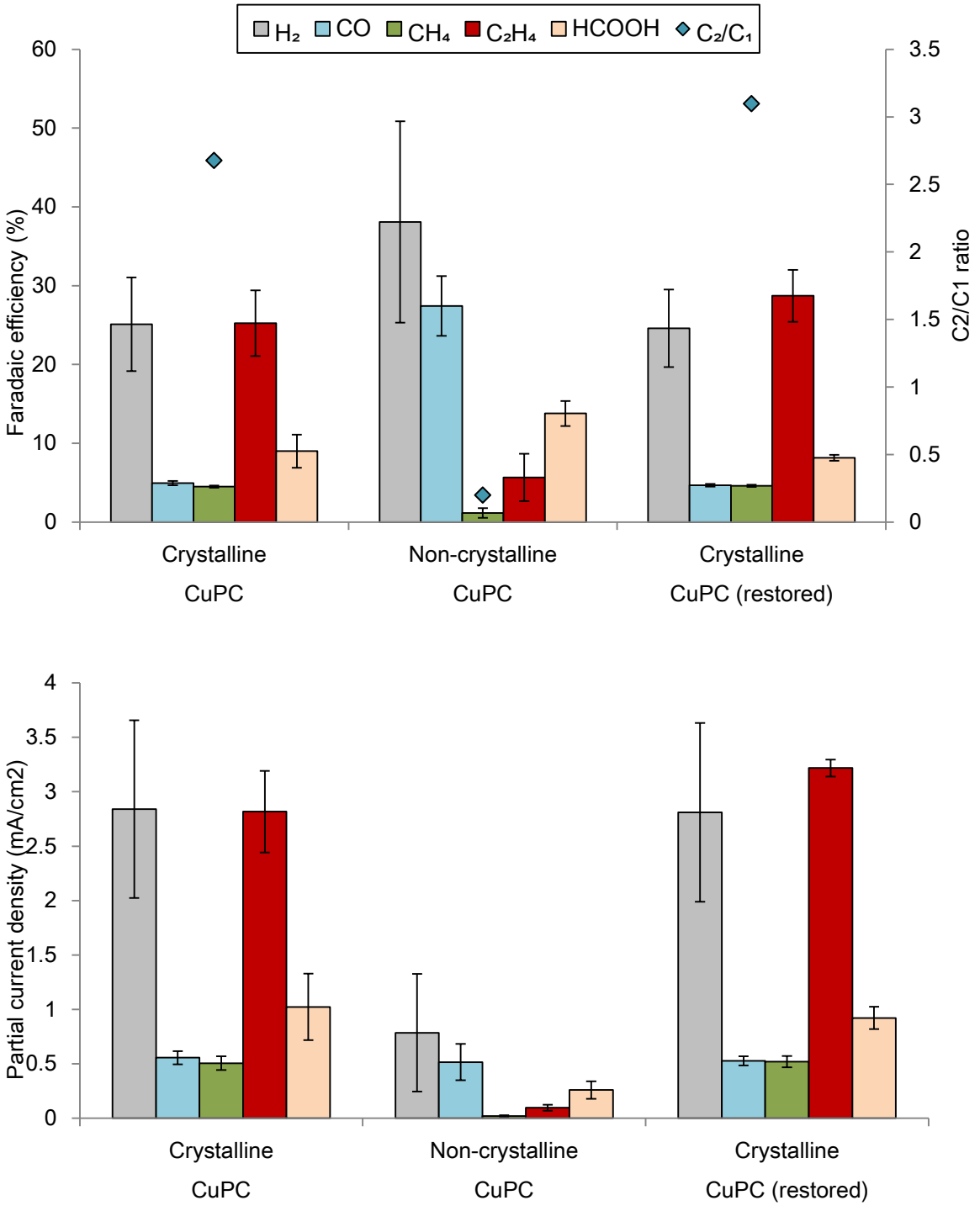

Figure S6. The overall distribution of the products from CO_2 reduction at -1.6 V vs Ag/AgCl in the two-compartment cell. Data are means ± SD (n=3).

Table S2.

Faradaic efficiency and partial current density of the products obtained from CO_2 reduction at -1.6V vs Ag/AgCl in in the two-compartment cell shown in Figure S6. Data are means ± SD (n=3).

Faradaic efficiency (%)

	H_2	CO	CH_4	C_2H_4	HCOOH
Crystalline CuPC	25 ± 5.9	5 ± 0.3	4 ± 0.1	25 ± 4.2	9 ± 2.1
Noncrystalline CuPC	38 ± 12.8	27 ± 3.8	1 ± 0.6	6 ± 3.0	14 ± 1.6
Crystalline CuPC (restored)	25 ± 4.9	5 ± 0.2	5 ± 0.1	29 ± 3.3	8 ± 0.4

Partial current density (mA/cm^2)

	H_2	CO	CH_4	C_2H_4	HCOOH
Crystalline CuPC	2.8 ± 0.8	0.6 ± 0.1	0.5 ± 0.1	2.8 ± 0.4	1.0 ± 0.3
Noncrystalline CuPC	0.8 ± 0.5	0.5 ± 0.2	0.0	0.1 ± 0.0	0.3 ± 0.1
Crystalline CuPC (restored)	2.8 ± 0.8	0.5 ± 0.0	0.5 ± 0.1	3.2 ± 0.1	0.9 ± 0.1

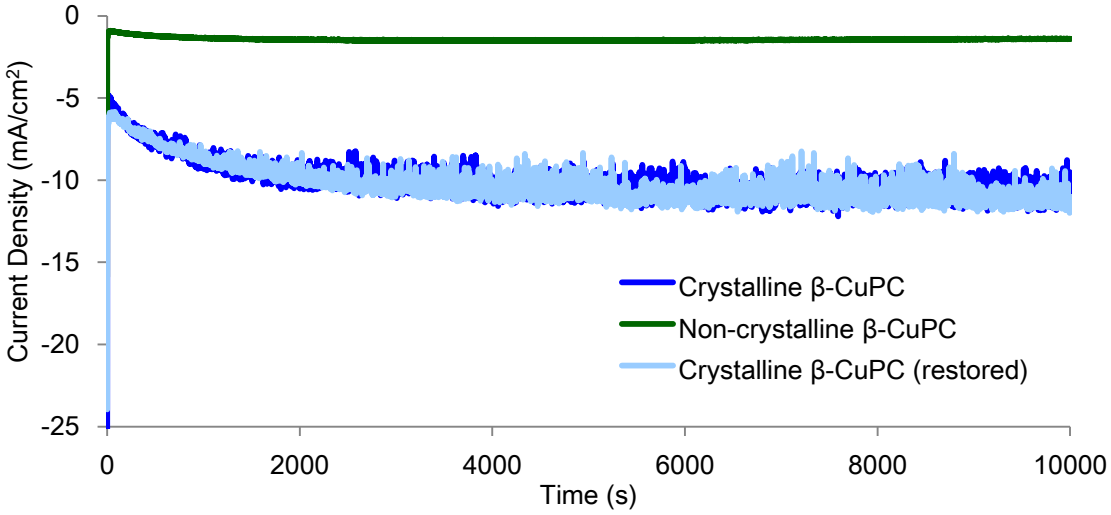

Figure S7. Total current density monitored during electrolysis at -1.6 V vs Ag/AgCl in the ordinary two-compartment cell shown in Figure 3.

(a)

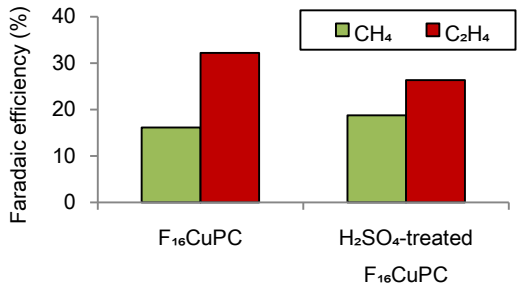
Faradaic efficiency (%)
40
30
20
10
0
CH4
C2H4
F16CuPC
H2SO4-treated F16CuPC

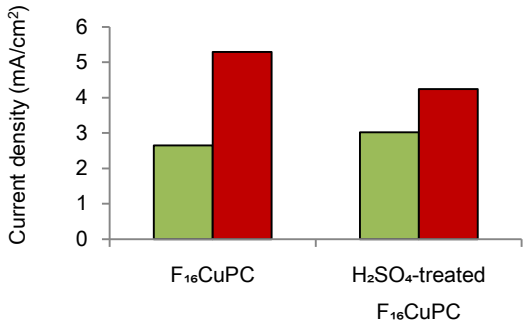
Current density (mA/cm2)
6
5
4
3
2
1
0
F16CuPC
H2SO4-treated F16CuPC

(b)

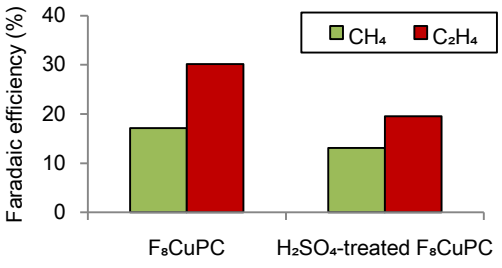
Faradaic efficiency (%)
40
30
20
10
0
CH4
C2H4
F8CuPC
H2SO4-treated F8CuPC

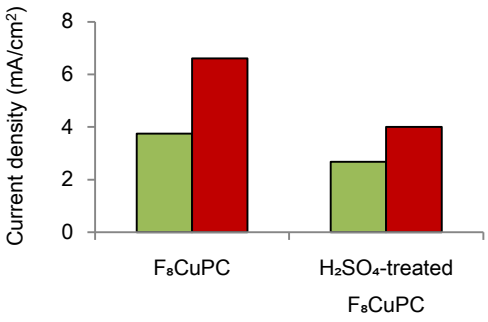
Current density (mA/cm2)
8
6
4
2
0
F8CuPC
H2SO4-treated F8CuPC

(c)

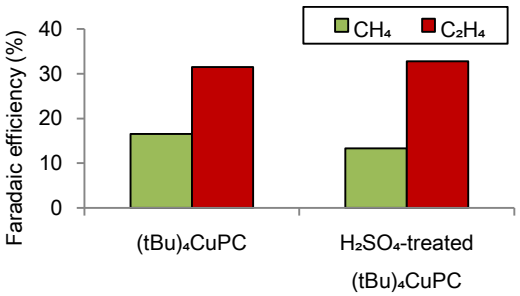
Faradaic efficiency (%)
40
30
20
10
0
CH4
C2H4
(tBu)4CuPC
H2SO4-treated (tBu)4CuPC

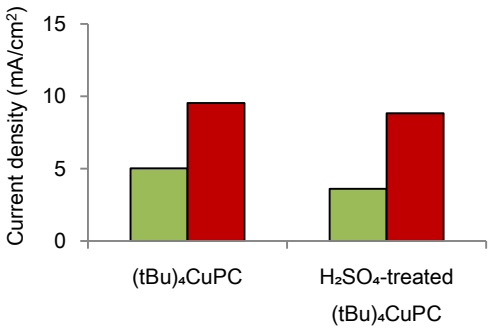
Current density (mA/cm2)
15
10
5
0
(tBu)4CuPC
H2SO4-treated (tBu)4CuPC

(d)

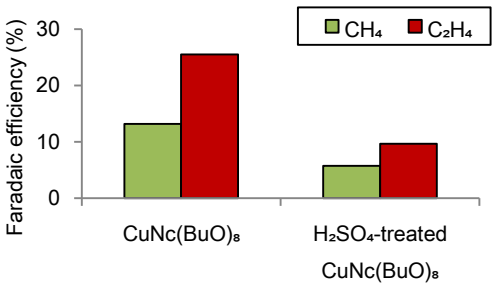
Faradaic efficiency (%)
30
20
10
0
CH4
C2H4
CuNc(BuO)8
H2SO4-treated CuNc(BuO)8

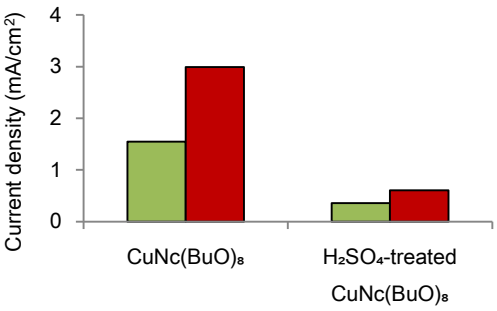
Current density (mA/cm2)
4
3
2
1
0
CuNc(BuO)8
H2SO4-treated CuNc(BuO)8

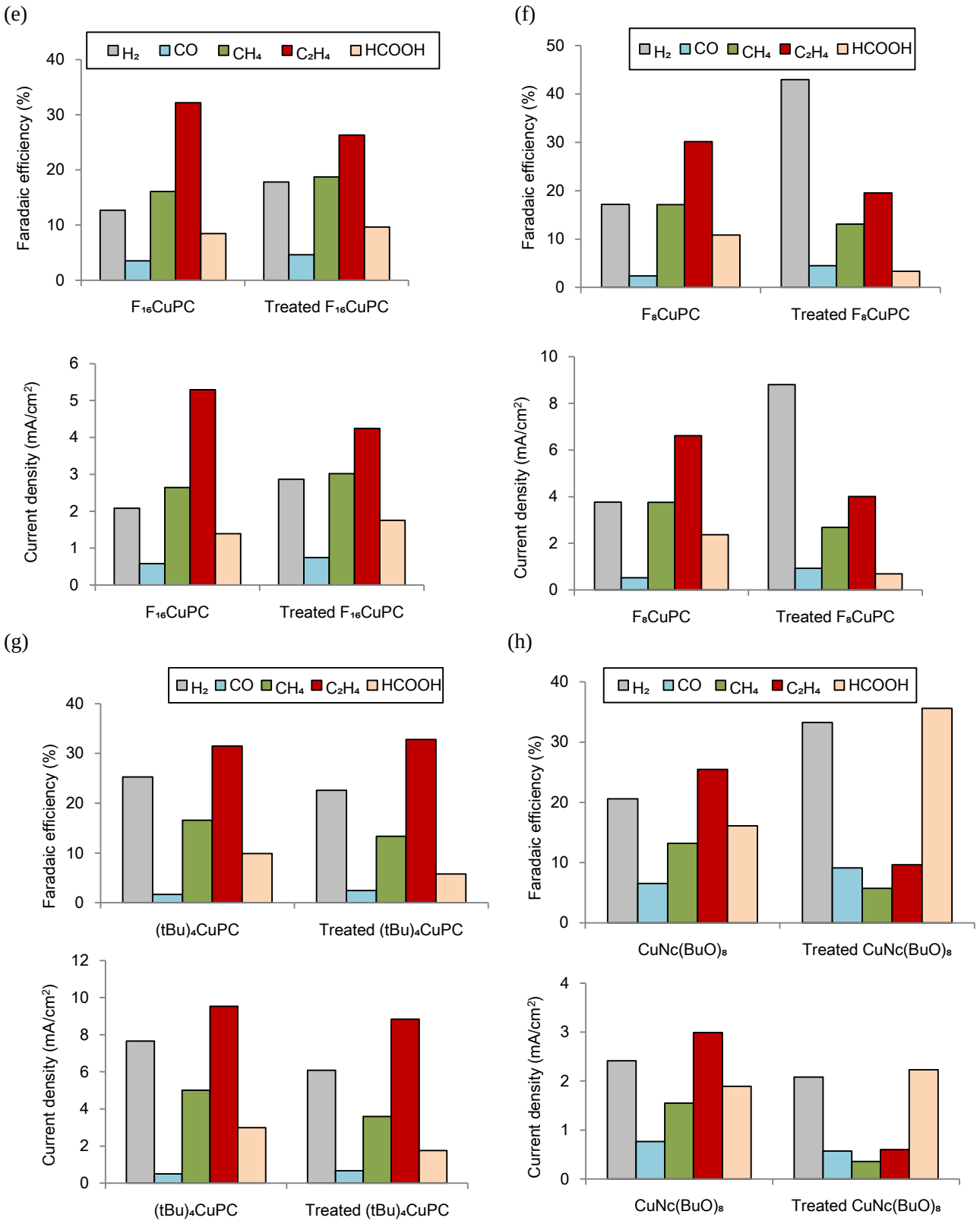

Figure S8. Faradaic efficiency and partial current density of C_2H_4 and CH_4 produced from CO_2 at -1.7 V vs Ag/AgCl using H_2SO_4-treated $F_{16}CuPc/C$ (a), F_8CuPc/C (b), $(tBu)_4CuPc/C$ (c), and $CuNC(BuO)_8/C$ (d). The overall distribution of the products from CO_2 reduction using H_2SO_4-treated $F_{16}CuPc/C$ (e), F_8CuPc/C (f), $(tBu)_4CuPc/C$ (g), and $CuNC(BuO)_8/C$ are also presented (h). Electrolysis was performed in the Combi-system.

(a)

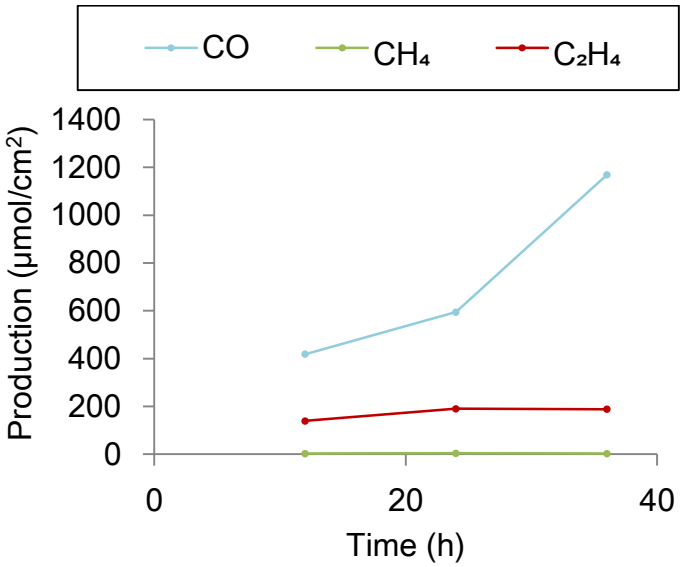

(b)

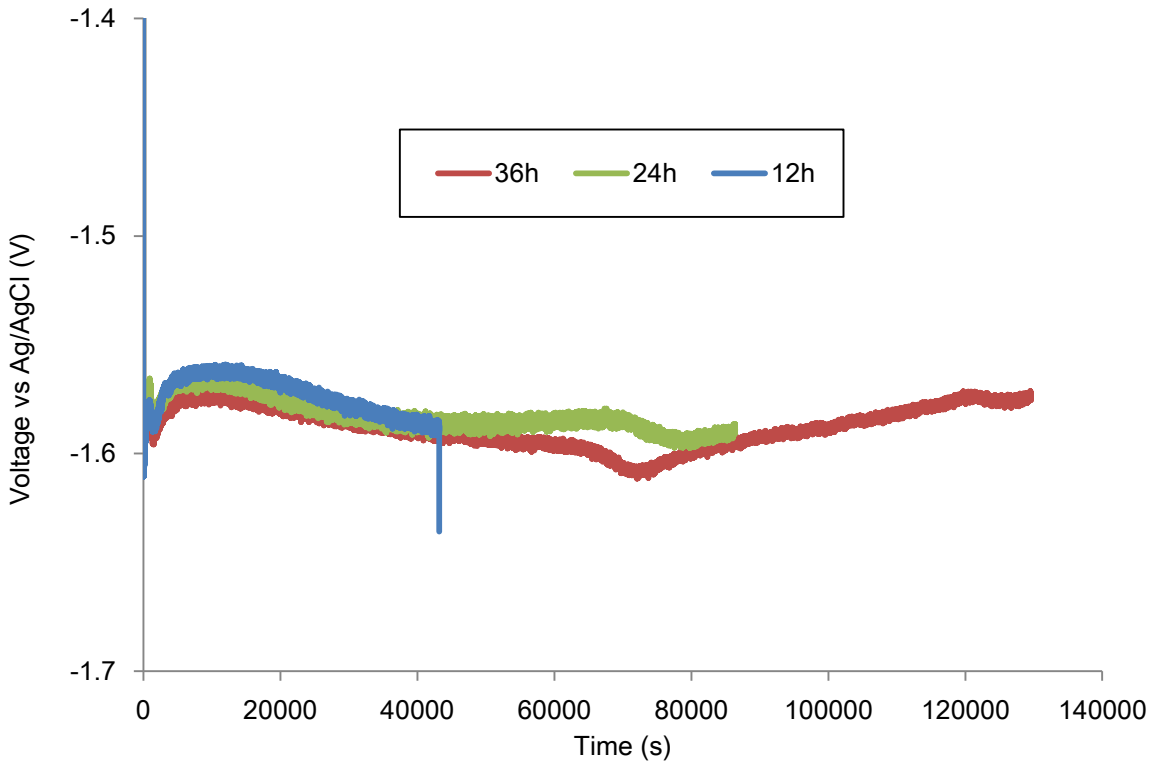

Figure S9. Products derived from CO_2 electrochemical reduction by crystalline CuPc/C at −11 mA/cm^2 in the Combi-system (a). Time-dependence fluctuations of potential vs Ag/AgCl during the electrolysis in the Combi-system (b).

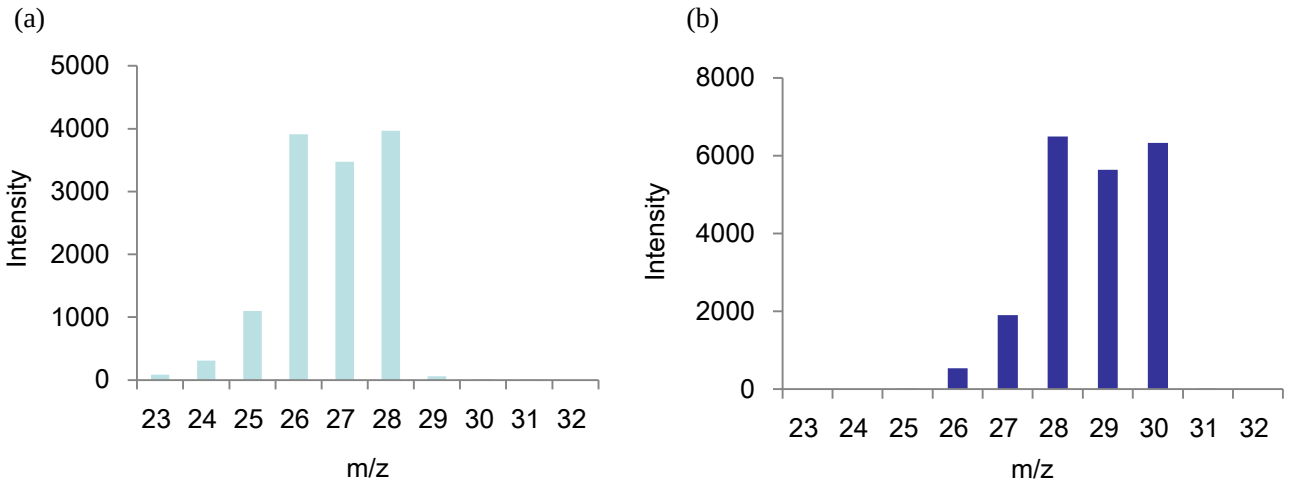

Figure S10. GC/MS spectra for C_2H_4 in gas phase after CO_2 reduction in $^{12}CO_2$- (a) and $^{13}CO_2$-saturated catholyte (b).

Carbon source was confirmed by GC/MS analysis of C_2H_4 in gas phase conducted after electrolysis. $^{12}C_2H_4$-peak at m/z = 28 and $^{13}C_2H_4$-peak at m/z = 30 were observed under $^{12}CO_2$ and $^{13}CO_2$ atmosphere, respectively, as well as respective fragmentary peaks. This indicates that carbon source of C_2H_4 produced in electrolysis was dissolved CO_2 in the electrolyte.

5. Measurements of C_{DL}, the electrochemical double-layer capacitance

Since we cannot measure the C_s, the capacitance of an atomically smooth planar surface of material per unit area under identical electrolyte conditions (see [McCrory et al. *JACS*. **2013**, 135 16977-16987), estimation of roughness factor is difficult. Thus, we measured and compared the values of C_{DL}, the electrochemical double-layer capacitance.

Below are shown cyclic voltammograms and double-layer charging current plotted against scan rates (Figure S11 and Table S3). In general, C_{DL} is believed to be accurate within an order of magnitude. Therefore, we conclude that active surface areas of the samples are not largely different within the accuracy of ESCA measurements.

(a)

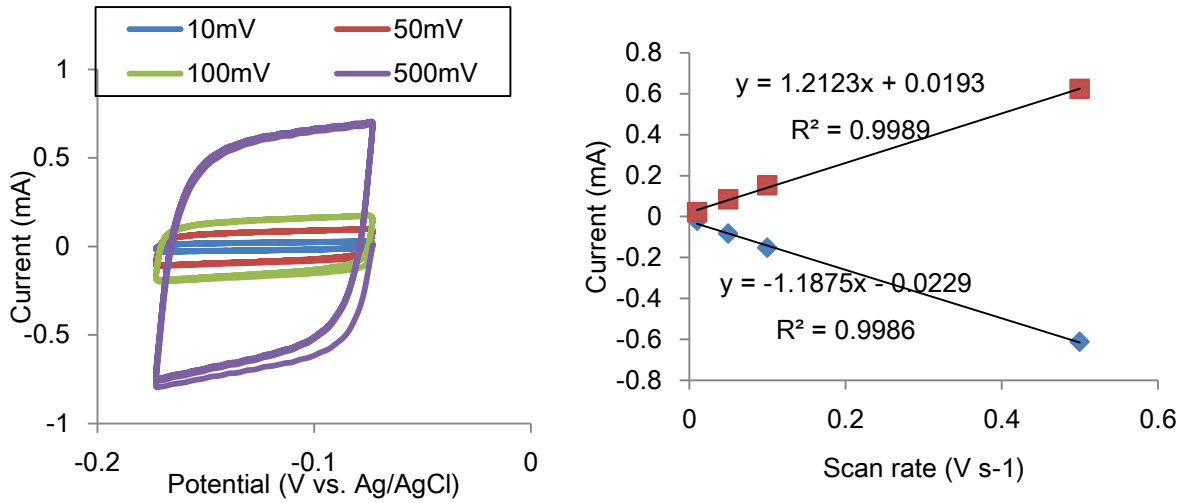

(b)

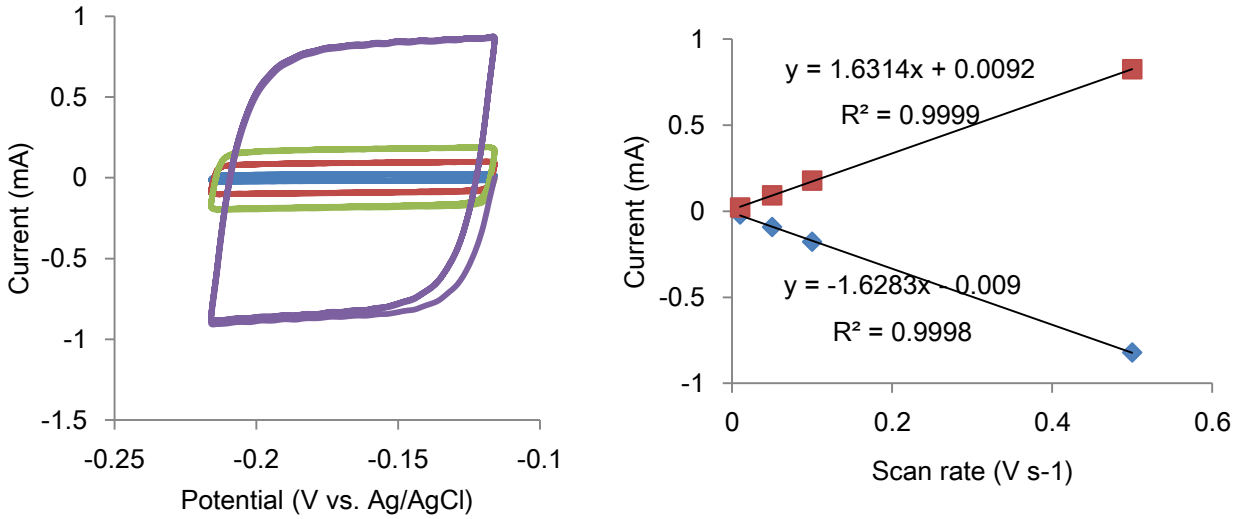

(c)

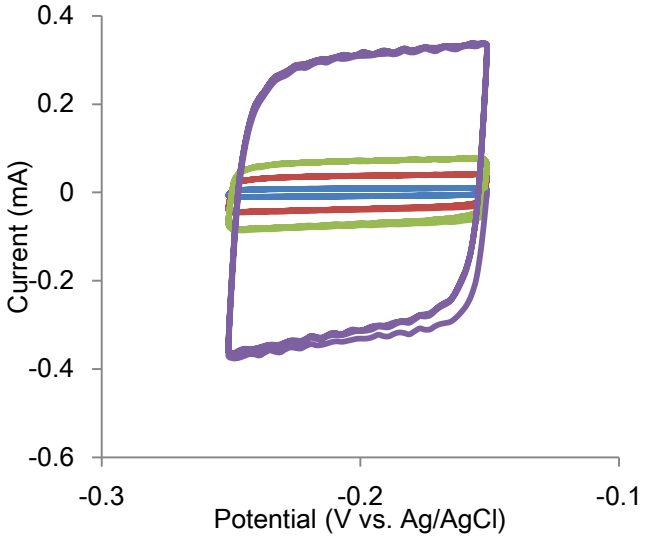
0.4
0.2
0
-0.2
-0.4
-0.6
Current (mA)
-0.3
-0.2
-0.1
Potential (V vs. Ag/AgCl)

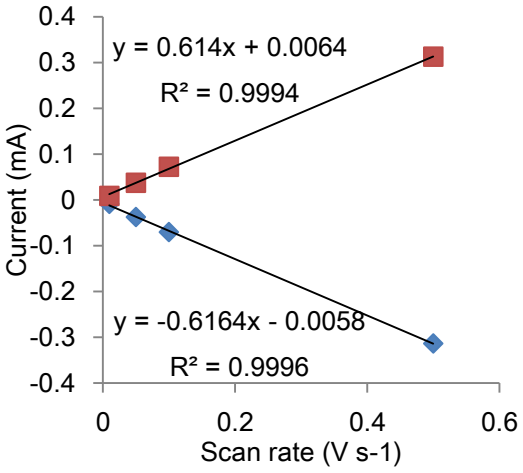
y = 0.614x + 0.0064
R² = 0.9994
y = -0.6164x - 0.0058
R² = 0.9996
Current (mA)
0.4
0.3
0.2
0.1
0
-0.1
-0.2
-0.3
-0.4
0
0.2
0.4
0.6
Scan rate (V s-1)

(d)

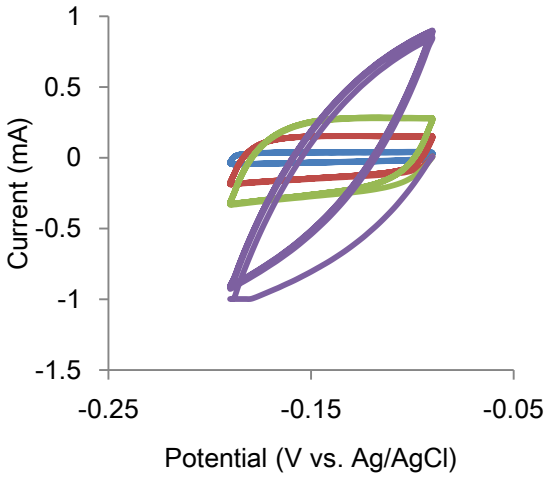
1
0.5
0
-0.5
-1
-1.5
Current (mA)
-0.25
-0.15
-0.05
Potential (V vs. Ag/AgCl)

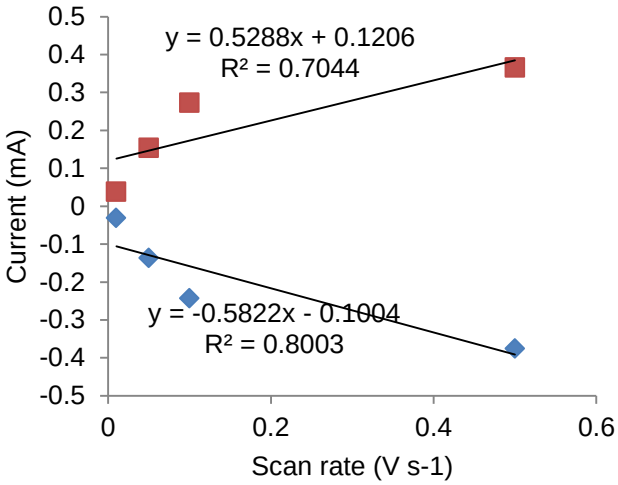
y = 0.5288x + 0.1206
R² = 0.7044
y = -0.5822x - 0.1004
R² = 0.8003
Current (mA)
0.5
0.4
0.3
0.2
0.1
0
-0.1
-0.2
-0.3
-0.4
-0.5
0
0.2
0.4
0.6
Scan rate (V s-1)

(e)

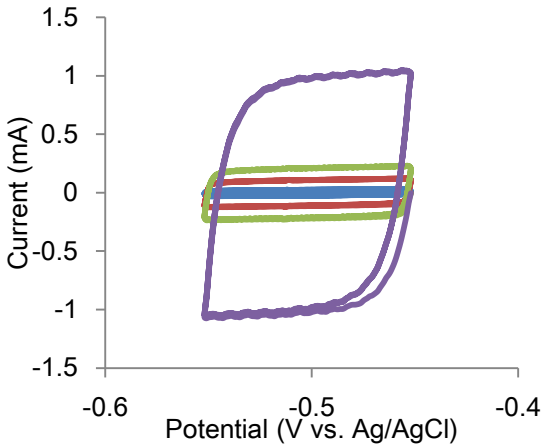
1.5
1
0.5
0
-0.5
-1
-1.5
Current (mA)
-0.6
-0.5
-0.4
Potential (V vs. Ag/AgCl)

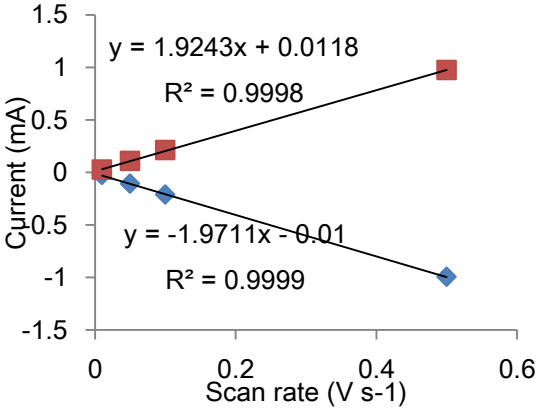
y = 1.9243x + 0.0118
R² = 0.9998
y = -1.9711x - 0.01
R² = 0.9999
Current (mA)
1.5
1
0.5
0
-0.5
-1
-1.5
0
0.2
0.4
0.6
Scan rate (V s-1)

(f)

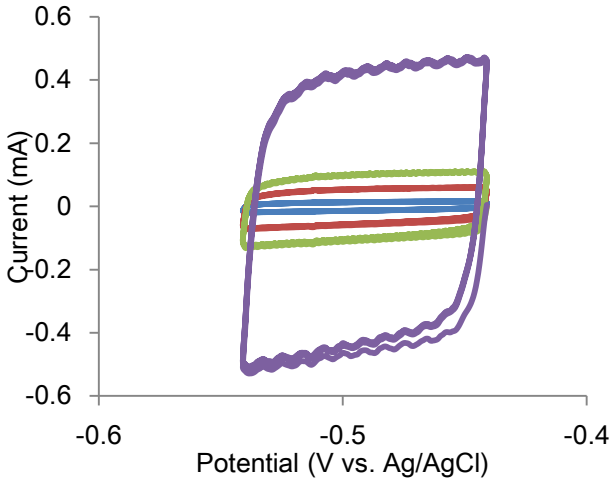
0.6
0.4
0.2
0
-0.2
-0.4
-0.6
Current (mA)
-0.6
-0.5
-0.4
Potential (V vs. Ag/AgCl)

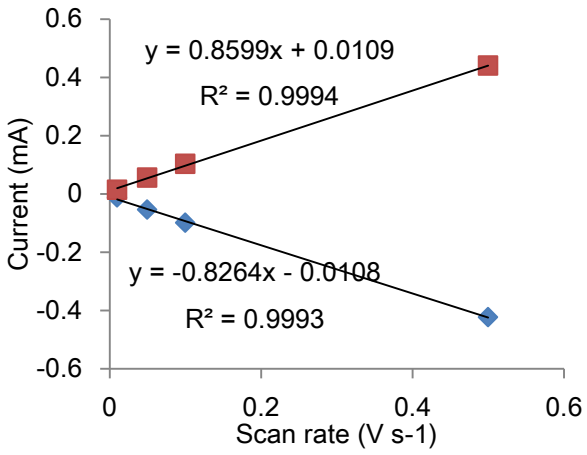
y = 0.8599x + 0.0109
R² = 0.9994
y = -0.8264x - 0.0108
R² = 0.9993
0.6
0.4
0.2
0
-0.2
-0.4
-0.6
Current (mA)
0
0.2
0.4
0.6
Scan rate (V s-1)

(g)

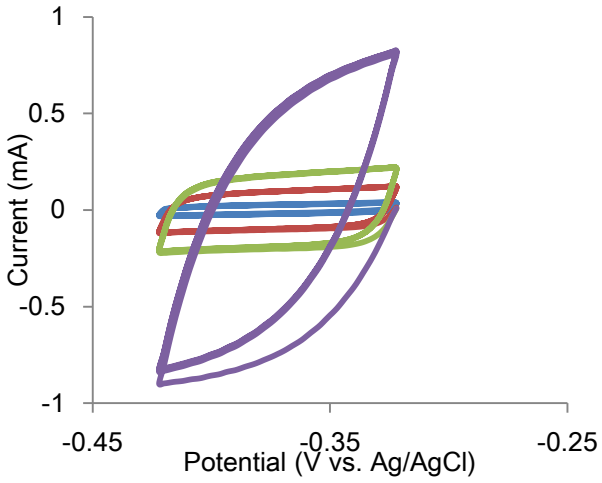
1
0.5
0
-0.5
-1
Current (mA)
-0.45
-0.35
-0.25
Potential (V vs. Ag/AgCl)

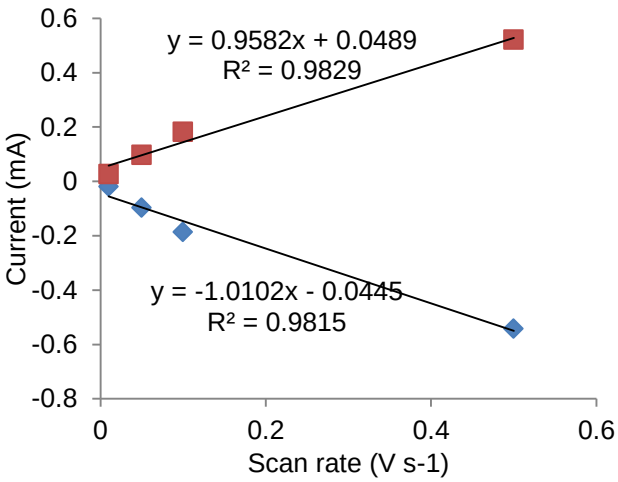
y = 0.9582x + 0.0489
R² = 0.9829
y = -1.0102x - 0.0445
R² = 0.9815
0.6
0.4
0.2
0
-0.2
-0.4
-0.6
-0.8
Current (mA)
0
0.2
0.4
0.6
Scan rate (V s-1)

(h)

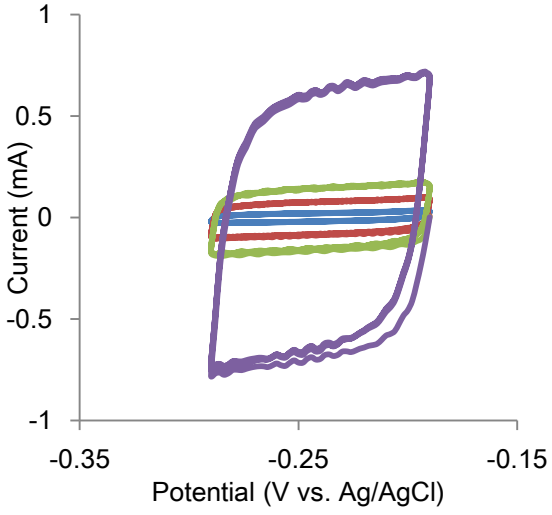
1
0.5
0
-0.5
-1
Current (mA)
-0.35
-0.25
-0.15
Potential (V vs. Ag/AgCl)

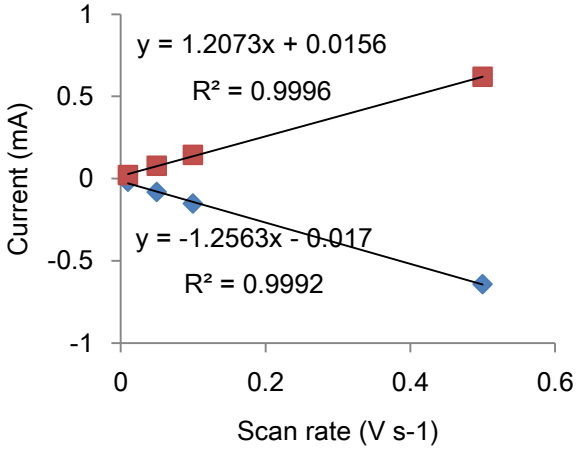
y = 1.2073x + 0.0156
R² = 0.9996
y = -1.2563x - 0.017
R² = 0.9992
1
0.5
0
-0.5
-1
Current (mA)
0
0.2
0.4
0.6
Scan rate (V s-1)

(i)

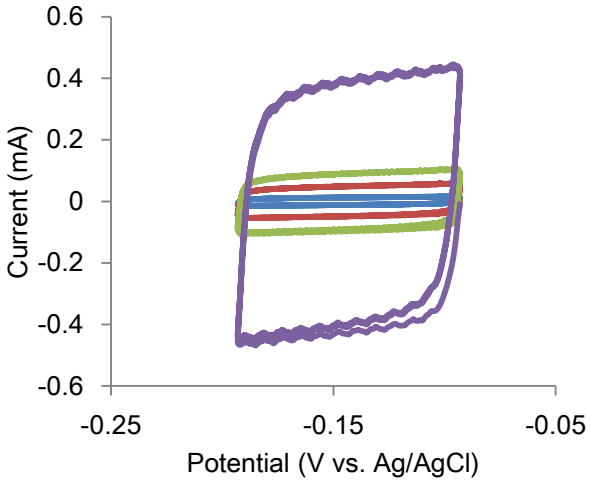
0.6
0.4
0.2
0
-0.2
-0.4
-0.6
Current (mA)
-0.25
-0.15
-0.05
Potential (V vs. Ag/AgCl)

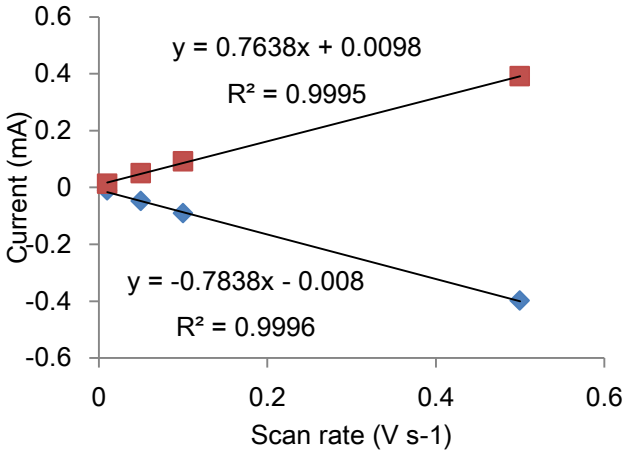
y = 0.7638x + 0.0098
R² = 0.9995
y = -0.7838x - 0.008
R² = 0.9996
Current (mA)
0
0.2
0.4
0.6
Scan rate (V s-1)

(j)

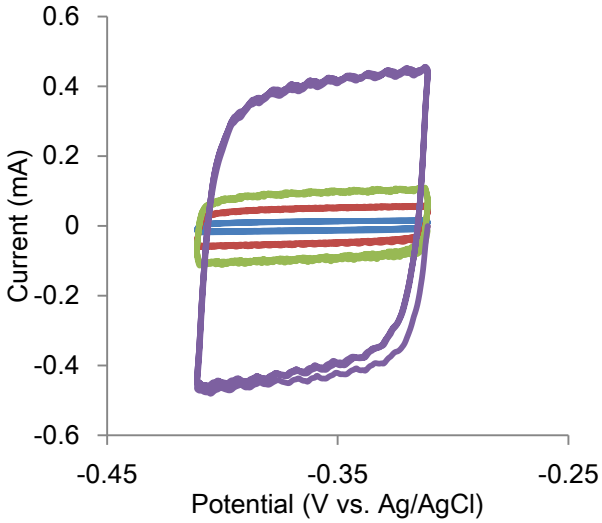
0.6
0.4
0.2
0
-0.2
-0.4
-0.6
Current (mA)
-0.45
-0.35
-0.25
Potential (V vs. Ag/AgCl)

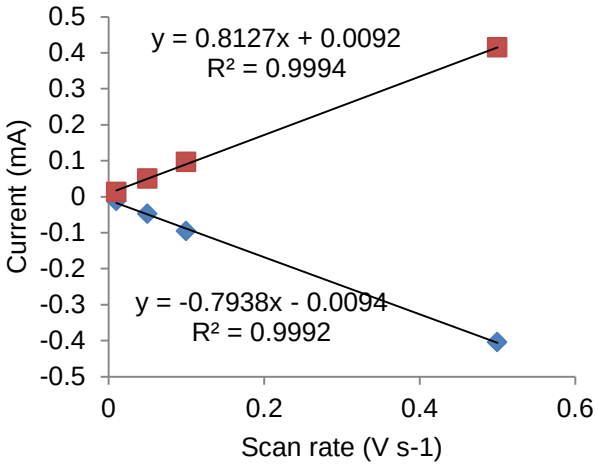
y = 0.8127x + 0.0092
R² = 0.9994
y = -0.7938x - 0.0094
R² = 0.9992
0.5
0.4
0.3
0.2
0.1
0
-0.1
-0.2
-0.3
-0.4
-0.5
Current (mA)
0
0.2
0.4
0.6
Scan rate (V s-1)

(k)

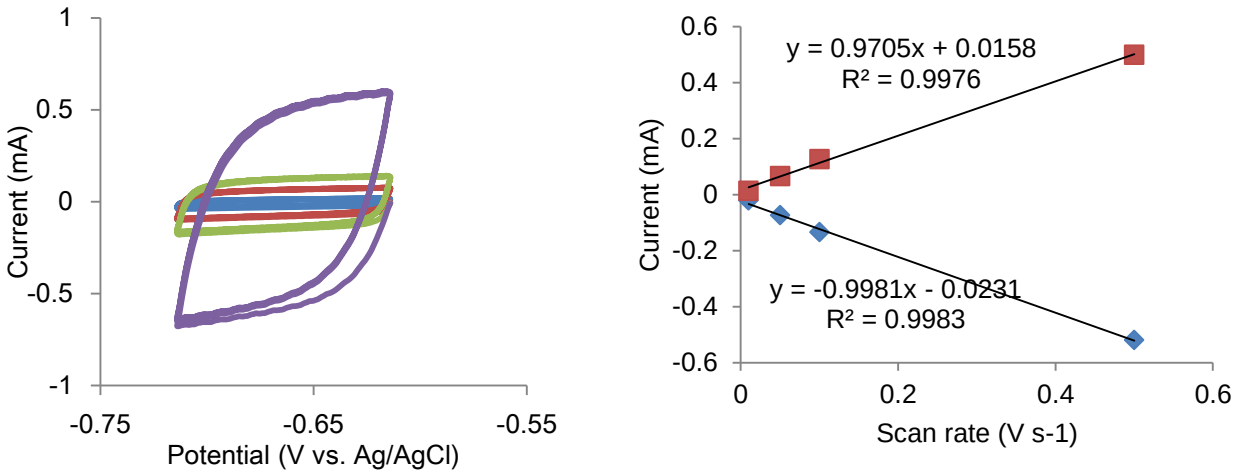

Figure S11. Cyclic voltammograms and double-layer charging current plotted against scan rates of crystalline CuPc (a), noncrystalline CuPc (b), crystalline CuPc (restored) (c), F_{16}CuPc (d), H_2SO_4-treated F_{16}CuPc (e), F_8CuPc (f), H_2SO_4-treated F_8CuPc (g), $(tBu)_4$CuPc (h), H_2SO_4-treated $(tBu)_4$CuPc (i), CuNc$(BuO)_8$ (j), and H_2SO_4-treated CuNc$(BuO)_8$ (k).

Table S3. Values of double-layer charging current (C_{DL})

Sample	C_{DL}
F_{16}CuPc	0.53
Treated F_{16}CuPc	1.9
F_8CuPc	0.84
Treated F_8CuPc	0.98
Crystalline β-CuPc	1.2
Noncrystalline β-CuPc	1.6
Crystalline β-CuPc (restored)	0.6
$(tBu)_4$CuPc	1.2
Treated $(tBu)_4$CuPc	0.77
CuNc$(BuO)_8$	0.80
Treated CuNc$(BuO)_8$	0.98

6. Confirmation of reproducibility

(a)

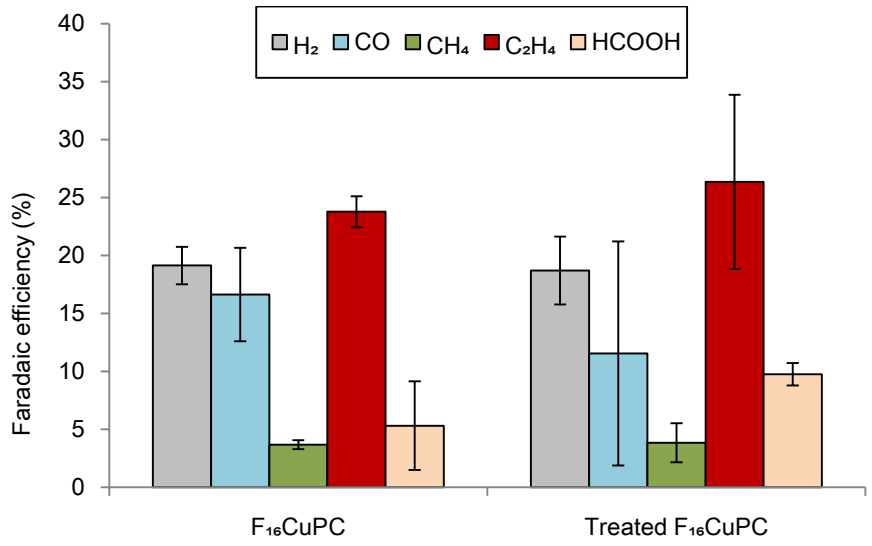

(b)

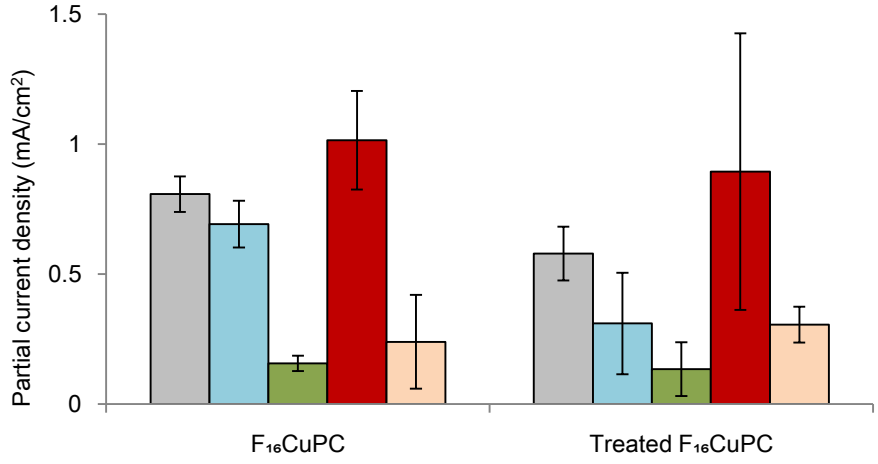

Figure S12. Confirmation of reproducibility of data shown in Figure S8(e).
Faradaic efficiency (a) and partial current density of H_2, CO, CH_4, C_2H_4 and HCOOH produced from CO_2 by F_{16}CuPc/C and H_2SO_4-treated F_{16}CuPc/C during 10,000sec-electrolysis at −1.6 V vs Ag/AgCl (b). Electrolysis was performed three times in the ordinary two-compartment H-cell. Values are means ±SD (n=3).

References

[1] McCrory, C. C.; Jung, S.; Peters, J. C.; Jaramillo, T. F.; *J. Am. Chem. Soc*. **2013**, *135*, 16977-16987.

[2] Hashiba, H.; Yotsuhashi, S.; Deguchi, M.; Yamada, Y. *ACS Comb. Sci*. **2016**, *18*, 203-208.